ChemComm

COMMUNICATION

View Article Online
View Journal | View Issue

Cite this: *Chem. Commun.*, 2018, **54**, 1331

Received 4th November 2017,
Accepted 25th December 2017

DOI: 10.1039/c7cc08505b

rsc.li/chemcomm

A versatile single molecular precursor for the synthesis of layered oxide cathode materials for Li-ion batteries†

Maofan Li, Jiajie Liu, Tongchao Liu, Mingjian Zhang* and Feng Pan*

A carbonyl-bridged single molecular precursor $LiTM(acac)_3$ [transition metal (TM) = cobalt/manganese/nickel (Co/Mn/Ni), acac = acetylacetone], featuring a one-dimensional chain structure, was designed and applied to achieve the layered oxide cathode materials: $LiTMO_2$ (TM = Ni/Mn/Co, NMC). As examples, layered oxides, primary $LiCoO_2$, binary $LiNi_{0.8}Co_{0.2}O_2$ and ternary $LiNi_{0.5}Mn_{0.3}Co_{0.2}O_2$ were successfully prepared to be used as cathode materials. When they are applied to lithium-ion batteries (LIBs), all exhibit good electrochemical performance because of their unique morphology and great uniformity of element distribution. This versatile precursor is predicted to accommodate many other metal cations, such as aluminum (Al^{3+}), iron (Fe^{2+}), and sodium (Na^+), because of the flexibility of organic ligand, which not only facilitates the doping-modification of the NMC system, but also enables synthesis of Na-ion layered oxides. This opens a new direction of research for the synthesis of high-performance layered oxide cathode materials for LIBs.

Layered oxide cathode materials, including lithium cobalt oxide ($LiCoO_2$) and its series derivatives: lithium (nickel, manganese, cobalt) oxygen [Li(Ni, Mn, Co)O_2; NMC], are the main options for the cathode materials of lithium ion batteries (LIBs). Industrial production of these materials has been implemented because of their good comprehensive performance, including large capacity, good cycling and rate capability.[1–4] Thus, $LiCoO_2$ is the first commercialized cathode material, and still shares the biggest market because of its high volumetric energy-density and easy preparation.[5] However, it also has some drawbacks, such as relatively low practical capacity (around 140 mA h g^{-1}), high cost because of the rarity of the Co source, and high toxicity of Co compared with Ni, Mn and iron (Fe).[6,7] So developing new cathode materials with a high comprehensive performance has attracted a lot of attention and effort. Doping and replacement of Co with other TM elements becomes one of the successful strategies to tailor and enhance the electrochemical performance of cathode materials. Based on $LiCoO_2$, ternary Ni–Co–Mn systems with different TM ratios have been developed. Thus, Ni substitution is used to improve the specific capacity with a low cost, and Mn substitution is used to enhance the structural stability of the layered oxide.[8,9] So, multiple TM substitutions provides a vast potential for enhancing the comprehensive electrochemical performance of layered materials.

The advantage of tailoring properties by multiple TM substitutions, brings with it another difficulty in implementing uniform distribution of multiple metal elements in such a complicated polynary layered oxide system. In the traditional solid state method, mixing a Li source and multiple TM sources by grinding or ball milling could not implement the great uniformity required for precursors on a nanometer or atomic scale. Therefore, it is much more difficult to achieve the uniform distribution of TM elements with Li because of their much lower thermal diffusivities than Li.[10,11] To solve this problem, a co-precipitation method was developed. It combines multiple TM elements into one compound, such as TM hydroxide,[12,13] TM carbonate,[14,15] or TM oxalates,[16] to implement the uniformity of the TM elemental distribution, and then mixes it with a Li-source to get layered oxides using high temperature calcination.

Inspired by the co-precipitation method, the best strategy to implement the uniform distribution of all metal elements is to combine all the involved metal elements (including Li and TM), with the correct ratios, in one single compound. This method is called the single molecular precursor method. Taking layered oxides, for example lithium transition metal oxide ($LiTMO_2$), it requires an appropriate ligand to combine the Li and the TM into one compound with Li/TM ratio of 1. Until now, there have only been five reports of the synthesis of cathode materials using a single molecular precursor method developed by Dikarev's group and Schneider's group. Two of them are the synthesis of layered $LiCoO_2$.[17,18] The other three are the synthesis of spinel $LiMn_2O_4$ and layered $LiFeO_2$.[19–21] As is known, the synthesis of polynary layered oxides involving multiple TM cations, using the single molecular precursor method and their electrochemical performance has never been demonstrated before. In addition, various organic ligands provide more choices than the limited inorganic precipitant (such as OH^-

School of Advanced Materials, Peking University, Peking University Shenzhen Graduate School, Shenzhen 518055, China. E-mail: zhangmj@pkusz.edu.cn, panfeng@pkusz.edu.cn

† Electronic supplementary information (ESI) available. See DOI: 10.1039/c7cc08505b

and Co_3^{2-}), which might be beneficial to the co-precipitation efficiency of multiple metal cations.[22,23]

In this work, a carbonyl-bridged single molecular precursor $LiTM(acac)_3$ (TM = Co/Mn/Ni, acac = acetylacetone) featuring a one dimensional (1D) chain structure, was designed and applied to achieve the layered oxide cathode materials $LiTMO_2$ (TM = Co/Mn/Ni) in this research. Acac as a carbonyl-rich ligand was chose to implement precise control of the metal element compositions in single molecular precursors to lead to the correct compositions and great uniformity in the final products. As representatives, layered oxides, $LiCoO_2$, $LiNi_{0.8}Co_{0.2}O_2$ and $LiNi_{0.5}Mn_{0.3}Co_{0.2}O_2$ were successfully prepared using their single molecular precursors ($LiCo(acac)_3$, $LiNi_{0.8}Co_{0.2}(acac)_3$ and $LiNi_{0.5}Mn_{0.3}Co_{0.2}(acac)_3$), respectively. They all exhibited good electrochemical performance because of their unique morphology and the great uniformity of the elemental distribution.

The single molecular precursors were synthesized using the solution reflux method (details in the ESI†). As shown in Fig. S2 (ESI†), $LiCo(acac)_3$, $Li(Ni_{0.8}Co_{0.2})(acac)_3$ and $Li(Ni_{0.5}Mn_{0.3}Co_{0.2})(acac)_3$ were colored pink, lavender and light grey, respectively, with different TM compositions. The powder X-ray diffraction (XRD) pattern of $LiCo(acac)_3$ is illustrated in Fig. 1a, which was consistent with a previous report.[1] The patterns of $LiNi_{0.8}Co_{0.2}(acac)_3$ and $LiNi_{0.5}Mn_{0.3}Co_{0.2}(acac)_3$ (Fig. 1b and c) were similar to that of $LiCo(acac)_3$, which indicated that they all crystallized in the same space group ($R\bar{3}c$). The inductively coupled plasma – atomic emission spectroscopy (ICP-AES) results (Table S1, ESI†) indicated that the elemental compositions of Li and the TMs were precisely controlled in the individual compounds as they were designed to be.

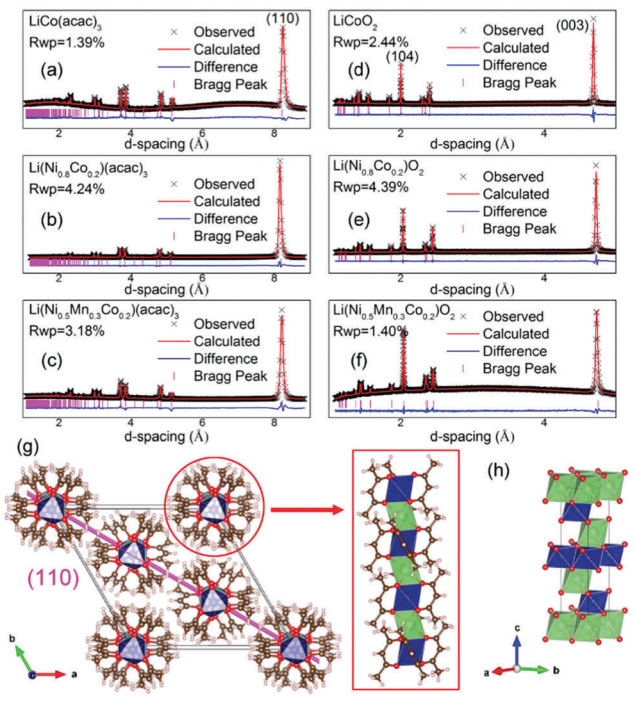

Fig. 1 Experimental XRD patterns of $LiCo(acac)_3$ (a), $Li(Ni_{0.8}Co_{0.2})(acac)_3$ (b) and $Li(Ni_{0.5}Mn_{0.3}Co_{0.2})(acac)_3$ (c), experimental XRD patterns of $LiCoO_2$ (d), $Li(Ni_{0.8}Co_{0.2})O_2$ (e) and $Li(Ni_{0.5}Mn_{0.3}Co_{0.2})O_2$ (f), representative structural sketch maps of $LiCo(acac)_3$ (g) and $LiCoO_2$ (h).

About 1% Li loss was observed after calcination. Their crystal structure is illustrated in Fig. 1g. As can be seen, it is constructed with a lot of parallel-aligned 1D chains along the *c* axis, which consisted of alternately connected LiO_6 and TMO_6 octahedra within a face-sharing mode. Therefore, each TMO_6 octahedron was composed of a TM cation chelated with three acac molecules, and one LiO_6 octahedron was composed of a Li ion bridged by six acac molecules. As shown in Fig. 1h, the LiO_6 and TMO_6 octahedra are the basic structural units required to produce the layered oxides ($LiTMO_2$).

To study the effect of TM compositions on the crystal structure, Rietveld refinements were performed for the three XRD patterns by using the reported $LiCo(acac)_3$ structure as the initial model structure, and the relevant crystallographic parameters are shown in Table S2 (ESI†) and Fig. S2 (ESI†). As shown in Fig. S2a (ESI†), the unit cell parameters, a and c, firstly decreased with 80% Co(II) substitution with Ni(II), then increased with a further 30% Ni(II) substitution with Mn(II). However, this unique structure reflected that the organic ligand (acac) presented a much higher flexibility than the inorganic anions, OH^- and CO_3^{2-}, which could accommodate a much larger variation of metal–O bond lengths and long angles by the deformation of the organic ligands. So it is the reason why the organic ligand could combine Li ions and various TM cations into one crystal framework. This characteristic also allowed other metal cations to enter into the framework, thereby providing great potential for doping with other elements.

The corresponding layered oxides $LiCoO_2$, $LiNi_{0.8}Co_{0.2}O_2$ and $LiNi_{0.5}Mn_{0.3}Co_{0.2}O_2$ were prepared by calcining the corresponding precursors under previously optimized conditions. Their structures were measured using powder XRD (Fig. 1d–f). All the diffraction peaks can be indexed to hexagonal $LiCoO_2$ ($R\bar{3}m$) with a layered structure (JCPDS no. 75-0532), revealing high phase purity for them. The (003) and (104) peaks of $LiNi_{0.8}Co_{0.2}O_2$ and $LiNi_{0.5}Mn_{0.3}Co_{0.2}O_2$ shifted to a higher *d*-spacing direction than $LiCoO_2$, indicating larger lattice parameters after Ni and Mn substitution. An integrated intensity ratio of (003) to (104) peaks (denoted as $I(003)/I(104)$) is usually adopted to roughly evaluate the cationic disordering in a layered structure.[2] In this research, high $I(003)/I(104)$ values for $LiCoO_2$ and $LiNi_{0.8}Co_{0.2}O_2$ (1.35 and 1.22, respectively), implied that there was much less Li/Ni disordering in their layered structure, which hinted at good electrochemical performance for them. Rietveld refinements were also performed for these three XRD patterns, and the relevant crystallographic parameters are shown in Table S3 (ESI†) and Fig. S2 (ESI†). As shown in Fig. S2b (ESI†), the lattice parameters, a and c, increased with the Ni and Mn substitution, which is consistent with a previous report. The occupancy of Ni at the 3b site [denoted as Ni(3b)] was another important indicator of the Li/Ni disordering. The low Ni(3b) value (0.0394) in Table S3 (ESI†) also predicted a good electrochemical performance for $LiNi_{0.8}Co_{0.2}O_2$.

The morphology of precursors and corresponding layered oxides were investigated using scanning electron microscopy (SEM) characterization. As shown in Fig. 2, all the precursors presented a prism like shape, with a length about 10–20 μm and a width about 2–4 μm. This morphology was consistent with their hexagonal crystal structure shown in Fig. 1g, because the crystals preferred to grow up along

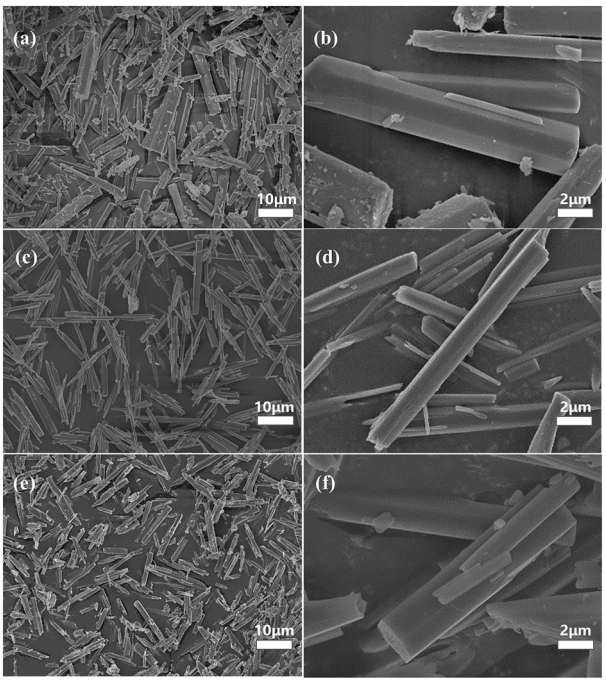

Fig. 2 Low magnification (a) and high magnification (b) SEM images of $LiCo(acac)_3$, low magnification (c) and high magnification (d) SEM images of $LiNi_{0.8}Co_{0.2}(acac)_3$, low magnification (e) and high magnification (f) SEM images of $LiNi_{0.5}Mn_{0.3}Co_{0.2}(acac)_3$.

the *c* axis by extending the 1D chain. The layered $LiCoO_2$ could be obtained using a very low temperature of 450 °C (Fig. S6, ESI†) with a particle size of around 200 nm (Fig. S7, ESI†). When calcined at a higher temperature (850 °C), the nanocrystals merged and grew significantly by about 10 times. As shown in Fig. 3a, a thick plate was composed by small particles with a size around 2 μm. The high-magnification SEM images in Fig. 3b showed the micrometer pillar shape with a surface exposed layered texture, a unique morphology for $LiCoO_2$ that has never been reported before. These surface exposed layered textures could be assigned to the (003) crystal plane according to its layered structure shown in Fig. 1h, which might be beneficial for Li^+ fast de/intercalation to enhance the rate capability. After sintering $LiNi_{0.8}Co_{0.2}(acac)_3$ at 800 °C for 8 h, $LiNi_{0.8}Co_{0.2}CoO_2$ presented a three-dimensional (3D) network framework composed of small particles (Fig. 3c) with a size of about 500 nm (Fig. 3d). As shown in Fig. 3e and f, $LiNi_{0.5}Mn_{0.3}Co_{0.2}O_2$ showed a similar 3D network morphology constructed with much smaller particles. The energy dispersive X-ray spectroscopy (EDX) elemental mapping was performed on three materials to study the elemental distribution of the TMs. Fig. S9 (ESI†) shows that Co, Mn and Ni were distributed uniformly in these samples. In addition, the chemical compositions of three single molecular precursors and the corresponding layered oxides were measured using ICP-AES (Table S1, ESI†). It is clear that the molar ratios of metal elements including Co, Li, Mn, and Ni were consistent with the pre-design. After calcination, the molar ratios of the metal elements were nearly constant. This further proved that the elemental composition could be precisely controlled by this single molecular precursor method.

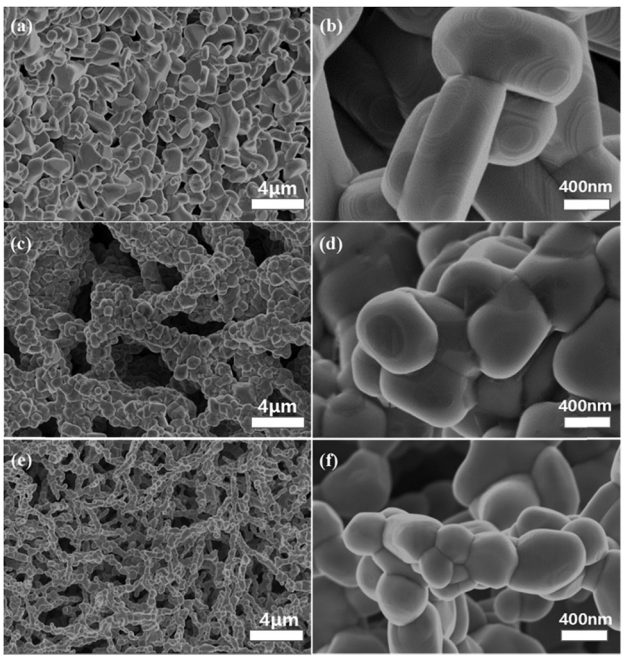

Fig. 3 Low magnification (a) and high magnification (b) SEM images of $LiCoO_2$, low magnification (c) and high magnification (d) SEM images of $LiNi_{0.8}Co_{0.2}O_2$, low magnification (e) and high magnification (f) SEM images of $LiNi_{0.5}Mn_{0.3}Co_{0.2}O_2$.

Finally, $LiCoO_2$, $LiNi_{0.8}Co_{0.2}O_2$ and $LiNi_{0.5}Mn_{0.3}Co_{0.2}O_2$ were assembled into half cells to test their electrode performance (see Experimental section in the ESI†). Fig. 4a shows the charge and discharge profiles of the first two cycles with a current density of 18 mA g^{-1} between 2.7 and 4.4 V for $LiCoO_2$. The 1st charge and discharge capacities were 180.9 and 171.3 mA h g^{-1}, and the capacities for the 2nd cycle were 170.5 and 170.1 mA h g^{-1}, respectively. The coulombic efficiencies for the 1st and 2nd cycles were calculated to be 94.6% and 99.7%, respectively. So the large capacities obtained were superior to those obtained for most of $LiCoO_2$ samples prepared by traditional solid state method and other methods.[24,25] The small capacity loss during the 1st cycle could be ascribed to the irreversible loss of Li ions caused by the formation of solid electrolyte interphase films. Fig. 4b shows the electrode capacities tested at the current densities increasing from 18 to 36, 90, 180, 360, 900, and 1800 mA g^{-1}, and five cycles were performed at each rate. The corresponding discharge capacities could reach 170, 165, 160, 155, 146, 128, and 86 mA h g^{-1}, respectively. The reversible capacity recovered to 163 mA h g^{-1} when the current density was brought back to 18 mA g^{-1}. Fig. 4c further illustrates the cycling performance of $LiCoO_2$ with a current density of 180 mA g^{-1} at 25 °C, which can retain a reversible capacity of 136.6 mA h g^{-1} with capacity retention of 88.7% after 50 cycles.

Similarly, Fig. 4d shows the charge and discharge profile of $LiNi_{0.8}Co_{0.2}O_2$ with a current density of 18 mA g^{-1}. It has charge and discharge capacities of 193.8 and 181.13 mA h g^{-1} for the 1st cycle, and 183.4 and 180.9 mA h g^{-1} for the 2nd cycle. Higher capacities and lower voltage plateaus were observed by comparing it with pure $LiCoO_2$ after Ni substitution, which was consistent with previous reports.[26,27] The coulombic efficiencies were also very high, 93.4% and 98.6% for the 1st and 2nd cycle, respectively. Fig. 4e shows an excellent rate capability, which was similar to that obtained with

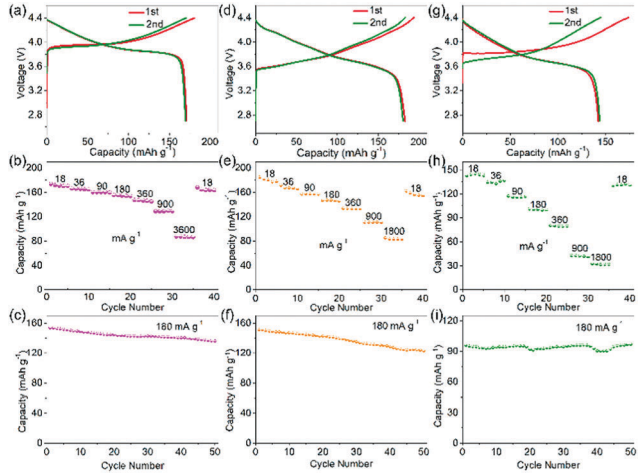

Fig. 4 Electrochemical performance of $LiCoO_2$, $LiNi_{0.8}Co_{0.2}O_2$ and $LiNi_{0.5}Mn_{0.3}Co_{0.2}O_2$. Charge and discharge profile at selected cycles with a current density of 18 mA g^{-1} for $LiCoO_2$ (a), $LiNi_{0.8}Co_{0.2}O_2$ (d) and $LiNi_{0.5}Mn_{0.3}Co_{0.2}O_2$ (g). Rate performance at various current densities for $LiCoO_2$ (b), $LiNi_{0.8}Co_{0.2}O_2$ (e) and $LiNi_{0.5}Mn_{0.3}Co_{0.2}O_2$ (h), and cycling performance with a current density of 180 mA g^{-1} at 25 °C for $LiCoO_2$ (c), $LiNi_{0.8}Co_{0.2}O_2$ (f) and $LiNi_{0.5}Mn_{0.3}Co_{0.2}O_2$ (i).

pure $LiCoO_2$. Fig. 4f further illustrates the cycling performance of $LiNi_{0.8}Co_{0.2}O_2$. The capacity retention was 81.5% after 50 cycles, which was lower than that of pure $LiCoO_2$. This might be because of the high Ni reactivity and structural reconstruction on the particle surface for high Ni layered oxides.[28] These excellent cycling results and rate performance could compare to, or were superior to, that obtained with $LiNi_{0.8}Co_{0.2}O_2$ prepared using a traditional solid state method or other methods.[29,30] Fig. 4g–i show the charge and discharge profiles, rate and cycling performance for $LiNi_{0.5}Mn_{0.3}Co_{0.2}O_2$, respectively. It was clear that the charge/discharge capacities decreased in comparison with $LiCoO_2$ and $LiNi_{0.8}Co_{0.2}O_2$ after Mn substitution. The rate performance also deteriorated after Mn substitution. Nevertheless, its cycling performance shown in Fig. 4i was greatly increased because of the Mn replacement. A super high capacity retention of 98.5% was obtained after 50 cycles. Thus, Mn substitution decreased the capacity and rate capability, but increased the cycling stability. This result is in agreement with the Mn's role in a layered oxide, *i.e.*, improving the structural stability.[9] In addition, the low capacity and poor rate capability might be because of the high Li/Ni mixing and small grain size as shown in Table S3 (ESI†).

In summary, multiple layered oxides ($LiTMO_2$), including $LiCoO_2$, $LiNi_{0.8}Co_{0.2}O_2$ and $LiNi_{0.5}Mn_{0.3}Co_{0.2}O_2$, were prepared using the thermal decomposition of a versatile precursor: $LiTM(acac)_3$. They not only presented a unique morphology with great uniformity of element distribution, but also exhibited good electrochemical performance. This provides a unique and valuable approach for preparing high performance electrode materials for LIBs. More layered cathode materials, such as nickel cobalt aluminum (NCA), and NCM with other TM ratios, even including layered sodium ion materials, are expected to be prepared using this method.

This work was supported by the Peacock Plan (KYPT2014-1016105435850), the Guangdong Innovative Research Team program (2013N080), the Chinese Postdoctoral Science Foundation (2015M570882, 2015M570894), the Shenzhen Science and Technology Research Grant (JCYJ20151015162256516, JCYJ20150729-111733470), the US Department of Energy (DOE) Office of Energy Efficiency and Renewable Energy under the Advanced Battery Materials Research (BMR) program (DE-SC0012704).

Conflicts of interest

There are no conflicts to declare.

Notes and references

1 N. A. Chernova, G. M. Nolis, F. O. Omenya, H. Zhou, Z. Li and M. S. Whittingham, *J. Mater. Chem.*, 2011, **21**, 9865–9875.
2 M. M. Thackeray, C. Wolverton and E. D. Isaacs, *Energy Environ. Sci.*, 2012, **5**, 7854–7863.
3 N. Nitta, F. X. Wu, J. T. Lee and G. Yushin, *Mater. Today*, 2015, **18**, 252–264.
4 M. D. Radin, S. Hy, M. Sina, C. Fang, H. Liu, J. Vinckeviciute, M. Zhang, M. S. Whittingham, Y. S. Meng and A. Van der Ven, *Adv. Energy Mater.*, 2017, **7**, 1602888.
5 K. Mizushima, P. C. Jones, P. J. Wiseman and J. B. Goodenough, *Mater. Res. Bull.*, 1980, **15**, 783–789.
6 E. M. Erickson, C. Ghanty and D. Aurbach, *J. Phys. Chem. Lett.*, 2014, **5**, 3313–3324.
7 B. L. Ellis, K. T. Lee and L. F. Nazar, *Chem. Mater.*, 2010, **22**, 691–714.
8 W. Liu, P. Oh, X. Liu, M. J. Lee, W. Cho, S. Chae, Y. Kim and J. Cho, *Angew. Chem., Int. Ed.*, 2015, **54**, 4440–4457.
9 A. Manthiram, J. C. Knight, S. T. Myung, S. M. Oh and Y. K. Sun, *Adv. Energy Mater.*, 2016, **6**, 1501010.
10 J. Li, R. Doig, H. S. Liu, G. Botton and J. R. Dahn, *J. Electrochem. Soc.*, 2016, **163**, A2841–A2848.
11 J. Li, R. Shunmugasundaram, R. Doig and J. R. Dahn, *Chem. Mater.*, 2016, **28**, 162–171.
12 X. M. Zhao, F. Zhou and J. R. Dahn, *J. Electrochem. Soc.*, 2008, **155**, A642–A647.
13 M. E. Spahr, P. Novak, B. Schnyder, O. Haas and R. Nesper, *J. Electrochem. Soc.*, 1998, **145**, 1113–1121.
14 L. Xu, P. Y. Hou, Y. T. Zhang, H. Z. Zhang, D. W. Song, X. X. Shi, X. Q. Wang and L. Q. Zhang, *J. Mater. Chem. A*, 2015, **3**, 21219–21226.
15 F. L. Liu, S. Zhang, C. Deng, Q. Wu, M. Zhang, F. L. Meng, H. Gao and Y. H. Sun, *J. Electrochem. Soc.*, 2012, **159**, A1591–A1597.
16 J. W. Kou, Z. Wang, L. Y. Bao, Y. F. Su, Y. Hu, L. Chen, S. Y. Xu, F. Chen, R. J. Chen, F. C. Sun and F. Wu, *Acta Phys.–Chim. Sin.*, 2016, **32**, 717–722.
17 Z. Wei, H. X. Han, A. S. Filatov and E. V. Dikarev, *Chem. Sci.*, 2014, **5**, 813–818.
18 J. Khanderi and J. J. Schneider, *Eur. J. Inorg. Chem.*, 2010, 4591–4594.
19 A. Navulla, L. Huynh, Z. Wei, A. S. Filatov and E. V. Dikarev, *J. Am. Chem. Soc.*, 2012, **134**, 5762–5765.
20 H. X. Han, Z. Wei, M. C. Barry, A. S. Filatov and E. V. Dikarev, *Dalton Trans.*, 2017, **46**, 5644–5649.
21 J. Khanderi and J. J. Schneider, *Inorg. Chim. Acta*, 2011, **370**, 254–259.
22 A. Bommel and J. R. Dahn, *Chem. Mater.*, 2009, **21**, 1500–1503.
23 H. Dong and G. M. Koenig Jr, *J. Mater. Chem. A*, 2017, **5**, 13785–13789.
24 Q. Cao, H. P. Zhang, G. J. Wang, Q. Xia, Y. P. Wu and H. Q. Wu, *Electrochem. Commun.*, 2007, **9**, 1228–1232.
25 Y. Takahashi, S. Tode, A. Kinoshita, H. Fujimoto, I. Nakane and S. Fujitani, *J. Electrochem. Soc.*, 2008, **155**, A537–A541.
26 X. X. Li, F. Y. Cheng, B. Guo and J. Chen, *J. Phys. Chem. B*, 2005, **109**, 14017–14024.
27 V. Etacheri, R. Marom, R. Elazari, G. Salitra and D. Aurbach, *Energy Environ. Sci.*, 2011, **4**, 3243–3262.
28 F. Lin, I. M. Markus, D. Nordlund, T. C. Weng, M. D. Asta, H. L. L. Xin and M. M. Doeff, *Nat. Commun.*, 2014, **5**, 3529.
29 C. Zhu, C. Yang, W. D. Yang, M. S. Wu, H. M. Ysai, C. Y. Hsieh and H. L. Fang, *J. Appl. Electrochem.*, 2010, **40**, 1665–1670.
30 L. F. Xiao, Y. Y. Yang, Y. Q. Zhao, X. P. Ai, H. X. Yang and Y. L. Cao, *Electrochim. Acta*, 2008, **53**, 3007–3012.

